JOURNAL OF PETROLOGY | VOLUME 45 | NUMBER 4 | PAGES 723–738 | 2004 | DOI: 10.1093/petrology/egg104

The Role of Open-System Processes in the Development of Silicic Magma Chambers: a Chemical and Isotopic Investigation of the Fogo A Trachyte Deposit, São Miguel, Azores

DARIN C. SNYDER[1]*, ELISABETH WIDOM[1], AARON J. PIETRUSZKA[2]† AND RICHARD W. CARLSON[2]

[1]DEPARTMENT OF GEOLOGY, MIAMI UNIVERSITY, OXFORD, OH 45056-1300, USA

[2]DEPARTMENT OF TERRESTRIAL MAGNETISM, CARNEGIE INSTITUTION OF WASHINGTON, 5241 BROAD BRANCH ROAD, NW, WASHINGTON, DC 20015, USA

RECEIVED SEPTEMBER 15, 2002; ACCEPTED AUGUST 18, 2003

The processes operating in the development of chemical zonation in silicic magma chambers have been addressed with a Sr–Nd–Pb–Hf–Th isotope study of the chemically zoned trachyte pumice deposit of the Fogo A eruption, Fogo volcano, Azores. Sr isotopic variation is observed in whole rocks, glass separates and sanidine phenocrysts (whole-rock $^{87}Sr/^{86}Sr$: 0·7049–0·7061; glass $^{87}Sr/^{86}Sr$: 0·7048–0·7052; sanidine $^{87}Sr/^{86}Sr$: 0·7048–0·7062). Thorium isotopic variation is observed in glass separates, with $(^{230}Th/^{232}Th)_o$ ranging from 0·8737 to 0·8841, and exhibiting a negative correlation with Sr isotopes. The Nd, Pb and Hf isotopic compositions of the whole-rock trachytic pumices are invariant and indistinguishable from basalts flanking the volcano. The Sr isotope variations in the whole rocks are proposed to be the result of three distinct processes: contamination of the Fogo A magma by assimilation of radiogenic seawater-altered syenite wall rock, to explain the Sr and Th isotopic compositions of the glass separates; incorporation of xenocrysts into the trachytic magma, required to explain the range in feldspar Sr isotopic compositions; and post-eruptive surface alteration. This study emphasizes the importance of determining the isotopic composition of glass and mineral separates rather than whole rocks when pre-eruptive magmatic processes are being investigated.

KEY WORDS: *Azores; open-system processes; Sr isotopes; trachytic pumices; zoned magma chambers*

INTRODUCTION

The products of many large explosive volcanic eruptions are chemically zoned. The process of zonation may generate highly evolved (e.g. trachytic or rhyolitic) and volatile-oversaturated magmas. Because volatile oversaturation is recognized as an important trigger of explosive volcanic eruptions (Blake, 1984), understanding the processes that lead to zonation and volatile oversaturation and the timescales over which these processes occur is important.

Chemical, as well as isotopic, zonation has been recognized in many large silicic volcanic deposits (Hildreth, 1981; Johnson, 1989). Chemical zonation within silicic magma chambers has commonly been attributed to processes such as fractional crystallization (Michael, 1983; Cameron & Cameron, 1986) or convection-driven thermogravitational diffusion (Hildreth, 1981). Other processes are required to explain isotopic zonation within magma chambers. Processes that can contribute to the development of intra-magma chamber isotopic gradients include *in situ* radioactive decay (Christensen & DePaolo, 1993), wall rock assimilation, hydrothermal fluid interaction (Hildreth *et al.*, 1984; Wörner *et al.*, 1985; Bindeman & Valley, 2001), and magma recharge/mixing (Eichelberger *et al.*, 2000).

*Corresponding author. Telephone: (513) 529-3217. Fax: (513) 529-1542. E-mail: snyderdc@muohio.edu

†Present address: Department of Geological Sciences, 5500 Campanile Drive, San Diego State University, San Diego, CA 92182, USA.

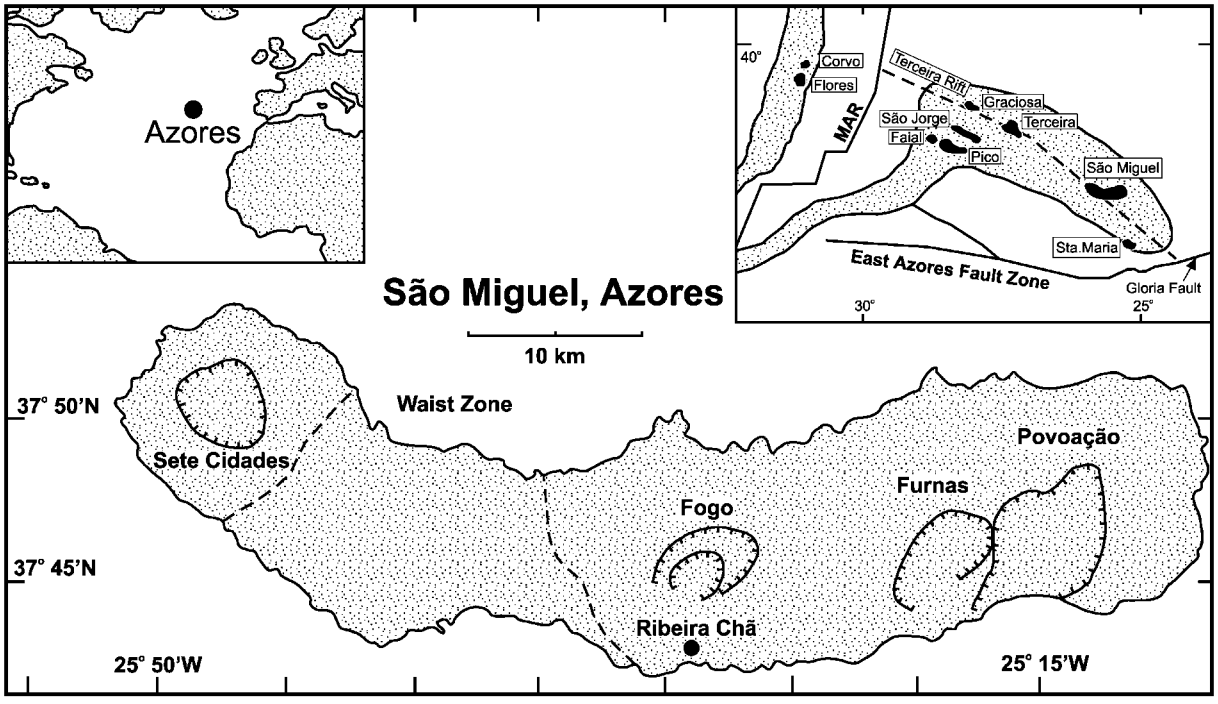

Fig. 1. A map showing the location of the Azores relative to the Mid-Atlantic Ridge (MAR), and a more detailed map of the island of São Miguel. São Miguel lies near the eastern end of the Azores platform, east of the MAR. The island comprises three large Quaternary stratovolcanoes: Fogo and Furnas (Povoação is extinct) in the east and Sete Cidades in the west (hachured lines mark calderas). The eastern and western stratovolcanoes are separated by two fields of Quaternary alkali basalt cinder cones and lava flows (Waist Zone above). After Moore (1990).

Although variations in Nd (Tegtmeyer & Farmer, 1990) and Pb (Wolff & Palacz, 1989) isotopic compositions have been reported in silicic volcanic deposits, silicic deposits are most commonly zoned with respect to Sr isotopic composition. The low Sr contents of these highly evolved systems give enormous leverage to almost any potential contaminant, be it mafic magma, sediment, or ocean spray. In contrast, Pb and Nd contents of such liquids are usually similar to, or greater than, those of potential contaminants. Hence, open-system processes often have little effect on Pb and Nd isotopic compositions, but significant effects on Sr isotopic compositions. Additionally, many highly evolved, low-Sr magmas have extremely high Rb/Sr ratios, allowing closed-system development of relatively high $^{87}Sr/^{86}Sr$ ratios. Prolonged magma residence times following magmatic fractionation events could thus produce significant variation in Sr isotope signatures. Determining which of these processes is responsible for the Sr isotopic variation has important implications for timescales of magmatic systems.

Christensen & DePaolo (1993) called upon dominantly closed-system processes to explain both the Sr isotopic zonation and the Sr isotopic disequilibrium displayed between feldspar phenocrysts and glass from the chemically zoned Bishop Tuff. Their model suggests that the increasing $^{87}Sr/^{86}Sr$ ratios in the glasses are primarily due to radioactive decay of ^{87}Rb in the high Rb/Sr liquids and requires a magma residence time between 300 and 500 kyr. However, magma residence time estimates based on Rb–Sr are dependent on the assumption of a closed system and are thus model dependent. More recent results based on U–Pb isotope analyses of zircons suggest that magmatic residence times for the early Bishop Tuff rhyolite are only a few tens of thousands of years (Reid & Coath, 2000).

This paper focuses on the isotopic characteristics of a chemically zoned trachytic pumice deposit in São Miguel, Azores, to assess the importance of open-system processes in the development of isotopic heterogeneities in zoned magma chambers. Sr, Nd, Pb, Hf and Th isotopic data, major and trace element data and field relationships allow for constraints to be placed on the pre-eruptive magma chamber processes. Our results show that whole-rock isotopic analyses combined with isotopic data on constituent materials (glass and phenocrysts) can provide fundamental information regarding the processes responsible for the isotopic zonation.

GEOLOGICAL SETTING

The Azores lie approximately 1400 km west of Portugal, straddling the Mid-Atlantic Ridge (MAR) between 37° and 40°N. The island of São Miguel is located near the eastern extent of the Azores platform (Fig. 1). São Miguel

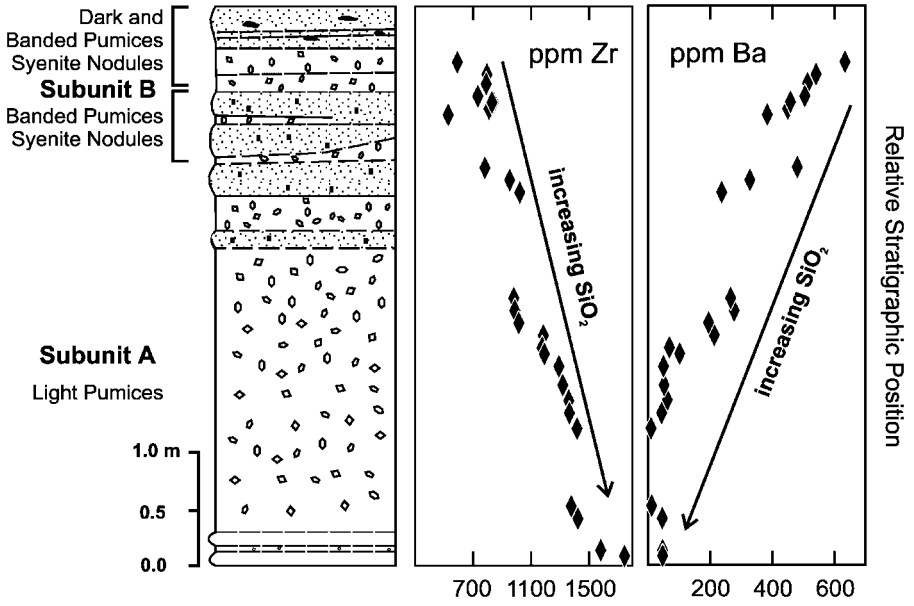

Fig. 2. A correlation exists between the major and trace element compositions of the trachytes and their stratigraphic position within the Fogo A deposit. The most evolved samples are located near the bottom of the deposit, with the samples becoming less evolved towards the top of the deposit. This zonation is interpreted to approximate the inverse compositional zonation of the pre-eruptive magma chamber.

has three active stratovolcanoes, Sete Cidades, Fogo and Furnas, that are separated by two fields of Quaternary alkali basalt cinder cones and lava flows (Booth *et al.*, 1978; Moore, 1990). The island is composed primarily of basaltic and trachytic rocks, although minor amounts of intermediate and mixed-magma hybrids have been identified (Storey *et al.*, 1989; Moore, 1991).

The Fogo volcano, located in the central portion of the island (Fig. 1), is composed of >90% trachytic pumice. The oldest dated unit is a 181 ka trachytic dome (Gandino *et al.*, 1985). The formation of the outer caldera took place between 46 and 26·5 ka, resulting in approximately 5 km^3 of welded and nonwelded pumice (Moore, 1990). The inner caldera forming eruption took place at about 15·2 ka, resulting in pumice-fall deposits and locally welded pyroclastic flows (Moore, 1990). No major eruptions occurred within the outer caldera for ~10–30 kyr between the formation of the inner and outer calderas. An additional hiatus in explosive activity of 10 kyr took place between formation of the inner caldera and eruption of the Fogo A deposit ~5 kyr ago (eleven ^{14}C ages range from 4·44 to 5·38 ka; Shotton *et al.*, 1968, 1969; Moore & Rubin, 1991). This paper focuses on the isotopic variations within the Fogo trachytic pumice and constrains the physical and chemical processes operating in the pre-eruptive magmatic system.

Fogo A deposit

The Fogo A deposit, first named and described by Walker & Croasdale (1970), was formed by a plinian eruption that produced 0·6–0·7 km^3 (dense rock equivalent) of trachytic pumice lapilli and ash. Additional surge and flow deposits were identified by Widom *et al.* (1992). The samples used in this study were collected from the area around Ribeira Chã. Although summarized here, a detailed description of the Fogo A deposit from the area around Ribeira Chã has been given by Widom *et al.* (1992). At this location, the total thickness of the deposit is about 5 m, and it can be texturally divided into two subunits (Fig. 2). Subunit A is about 3 m thick and forms 70–80% of the total erupted volume (Walker & Croasdale, 1970). The dominant constituent is light colored pumice grading upwards into darker and denser pumice (Bursik *et al.*, 1992). A maximum pumice size of 40 cm is observed about 250 cm above the base where the first syenite xenoliths and banded pumices occur (Widom *et al.*, 1992). Subunit B is about 1·5 m thick and contains three major surge horizons (Widom *et al.*, 1992). Large syenite xenoliths and banded pumices become abundant about 90 cm above the lowermost surge horizon. The petrogenesis of these xenoliths has been detailed by Widom *et al.* (1993). The syenites are miarolitic with up to 10% void space. Fresh nodules have subhedral granular textures with interlocking sanidine crystals, whereas plutonically altered syenites are subhedral to anhedral granular with sanidine and perthite crystals forming interdigitating boundaries (Widom *et al.*, 1993).

Widom *et al.* (1992) provided a detailed model for the petrogenetic evolution of the Fogo A magmatic system through the use of chemical, textural, and U-series isotopic data. Major and trace element variations from

throughout the stratigraphic extent of the Fogo A deposit indicate that the trachytes represent the inverted, extrusive equivalent of a chemically zoned magma chamber (Fig. 2). Fractional crystallization models using the observed phenocryst phases suggest that the observed chemical zonation was achieved via 70–75% crystallization.

SAMPLES AND ANALYTICAL TECHNIQUES

Seven trachytic pumice samples were selected for whole-rock Sr, Nd, Pb and Hf isotopic analyses to best represent the chemical diversity of the Fogo A deposit. The trachytic pumices have 0·79–2·05 wt % CaO and 60·90–62·90 wt % SiO_2, and have widely varying trace element concentrations (e.g. Zr 791–1417 ppm; Ba 9–514 ppm; Sr 3–478 ppm; Widom *et al.*, 1992). These samples were powdered using a Spex alumina shatterbox. Six glass separates, also chosen to best represent the chemical diversity of the deposit, were analyzed for Sr and Th isotopic compositions. The glass was separated from the whole rock by hand picking under a binocular microscope, avoiding any apparent impurities. No secondary alteration products were observed in any of the material during this procedure. Glass separates were rinsed in methanol then cleaned with 2N HCl for 10 min in an ultrasonic bath followed by a rinse in high-purity water to remove any adhering salts. Individual sanidine phenocrysts from uncrushed whole-rock pumices were hand picked using a binocular microscope. Sanidines were obtained from whole rocks spanning much of the observed range in Sr isotopic composition. The size and abundance of phenocrysts were controlling factors for which pumices were chosen for sanidine extraction. Petrographic examination of the pumices indicates that <5% of the feldspar phenocrysts are perthitic; all are subhedral to euhedral and appear fully disaggregated. Prior to digestion, the individual crystals were cleaned with 2·5N HCl in an ultrasonic bath for ~45 s, then rinsed thoroughly in high-purity water to remove any salts from the surface of the crystals. Twelve whole-rock syenite xenoliths from the Fogo A deposit were rinsed in high-purity water, powdered using a Spex alumina shatterbox, and analyzed for Sr isotopic compositions.

All chemical separations and isotopic measurements were carried out at the Department of Terrestrial Magnetism. Whole-rock powders and sanidine separates were dissolved in Savillex vials in concentrated HF–HNO_3, to eventually be taken up in HBr (for Pb) or HCl (for Sr only). Pb was first separated from the samples following the procedure described by Walker *et al.* (1989). All material eluted before the Pb cut was kept for further separation of Rb, Sr, Nd and Hf. Separation of these elements involved the column procedure described by Walker *et al.* (1989), with the exception that the sample was loaded in 1N HCl–0·1N HF and the Hf eluted immediately using 10 ml of this acid mixture. Hf was further purified using an anion column procedure similar to the second column procedure described by Blichert-Toft *et al.* (1997). Separation of Ti from Hf was accomplished by placing the Hf cut from the second column back on the first cation column in 2·5N HCl with 50 μl of H_2O_2, eluting the Ti with 24 ml of 2·5N HCl, then eluting the Hf with 2·5N HCl–0·3N HF. Sm–Nd separation for whole rocks was accomplished using hydrogen-diethyl-hexyl-phosphate (HDEHP) columns. Sr was separated from single sanidine crystals using Eichrom Sr resin following procedures similar to those of Deniel & Pin (2001). Sr, Th and U were separated from glass following the procedure described by Pietruszka *et al.* (2002), with the exception that the Th and U cuts for isotopic composition were passed through a second 50 μl column of Eichrom TRU (TransUranic) Resin to remove potential high-mass hydrocarbon interferences.

The isotopic compositions and concentrations of strontium by isotope dilution were measured by thermal ionization mass spectrometry (TIMS) on a VG-354 system. Strontium isotope ratios are corrected for fractionation using $^{86}Sr/^{88}Sr = 0{\cdot}1194$. All isotopic measurements assume an exponential mass dependence of the fractionation. All errors reported for isotopic measurements are 2 standard deviations of the mean. The reported values are normalized to a value of $^{87}Sr/^{86}Sr = 0{\cdot}71025$ for the NBS 987 standard. Measurements of this standard show a long-term reproducibility of ±0·000024 about a mean of 0·710281. Neodymium, Hf, Pb and Th isotopic compositions and Rb, Nd, Sm, Hf, Pb and Th concentrations by isotope dilution were measured by inductively coupled plasma mass spectrometry (ICP-MS) on a VG-P54 multi-collector (MC) system. Neodymium and Hf were measured statically. Hafnium is fractionation corrected to $^{178}Hf/^{177}Hf = 0{\cdot}7325$ and reported relative to a value of $^{176}Hf/^{177}Hf = 0{\cdot}282160$ for the JMC475 standard. Nine measurements of this standard provide an average value of $^{176}Hf/^{177}Hf = 0{\cdot}282152 \pm 0{\cdot}000011$. Neodymium is fractionation corrected to $^{146}Nd/^{144}Nd = 0{\cdot}7219$ and normalized to the La Jolla value of $^{143}Nd/^{144}Nd = 0{\cdot}51186$. Fifteen measurements of this standard provided a mean value of $0{\cdot}511855 \pm 0{\cdot}000118$ during the course of this study. However, 4–6 repeat measurements of this standard during individual analytical sessions indicate a much better precision of ±0·000020. Therefore, the Nd data reported here are corrected to the average value determined for 4–6 repeat analyses of the La Jolla standard run on the same day as the samples. Lead isotopic compositions were measured statically on the VG-P54 system, using the thallium addition method

for fractionation correction (e.g. Rehkamper & Halliday, 1998). Our overall precision for Tl-spiked Pb measurements as determined for 16 repeats of the NIST 981 standard value is $^{206}Pb/^{204}Pb = 0{\cdot}14\%$, $^{207}Pb/^{204}Pb = 0{\cdot}17\%$ and $^{208}Pb/^{204}Pb = 0{\cdot}30\%$, approximately the same as we achieve for thermal ionization analysis of Pb. Within one analytical session, however, the fractionation of Tl and Pb track one another much better, as indicated by precision of five repeat measurements of NIST 981 of $^{206}Pb/^{204}Pb = 0{\cdot}06\%$, $^{207}Pb/^{204}Pb = 0{\cdot}07\%$ and $^{208}Pb/^{204}Pb = 0{\cdot}15\%$. Consequently, we normalize the sample Pb data reported here to the average value determined for 2–5 repeat analyses of NIST 981 run on the same day as the samples. After this correction, the data are normalized to the NIST 981 values of $^{206}Pb/^{204}Pb = 16{\cdot}9356$, $^{207}Pb/^{204}Pb = 15{\cdot}4891$ and $^{208}Pb/^{204}Pb = 36{\cdot}7006$ as reported by Todt *et al.* (1996). The Th and U concentrations and isotope ratios were measured using the high-precision isotope dilution MC-ICP-MS technique described by Pietruszka *et al.* (2002). Th/U, ($^{234}U/^{238}U$) and ($^{232}Th/^{230}Th$) ratio measurements of the Pliocene rock standard TML (Jar #3) show a long-term reproducibility of $\pm 0{\cdot}06\%$, $\pm 0{\cdot}19\%$ and $\pm 0{\cdot}23\%$ 2σ, respectively (Pietruszka *et al.*, 2002).

RESULTS

Whole-rock trachytic pumices

The seven whole-rock trachytic pumices display a wide range of $^{87}Sr/^{86}Sr$ (0·7049–0·7062) but a narrow range of $^{143}Nd/^{144}Nd$ (0·51272–0·51274), $^{176}Hf/^{177}Hf$ (0·28280–0·28281) and $^{206}Pb/^{204}Pb$ (19·92–19·98) isotope ratios (Table 1). The Nd and Pb isotopic compositions of the whole rocks are within the range of those reported by Widom *et al.* (1997) for basalts flanking Fogo volcano ($^{143}Nd/^{144}Nd = 0{\cdot}51273$–$0{\cdot}51280$ and $^{206}Pb/^{204}Pb = 19{\cdot}83$–$19{\cdot}91$), whereas the range in Sr isotopic compositions of the whole rocks extends to more radiogenic values than those of the flanking basalts ($^{87}Sr/^{86}Sr = 0{\cdot}7046$–$0{\cdot}7055$) (Fig. 3). The $^{87}Sr/^{86}Sr$ ratios in the Fogo A whole rocks exhibit an inverse correlation with Sr concentration (Fig. 4), with the most differentiated (lowest Sr concentrations) samples exhibiting the highest $^{87}Sr/^{86}Sr$ ratios.

Whole-rock syenite xenoliths strontium isotope compositions

Measured whole-rock Sr isotopic compositions and Sr concentrations for syenite xenoliths are reported in Table 1. The $^{87}Sr/^{86}Sr$ ratios of 12 whole-rock powders range from 0·7048 to 0·7067. The most radiogenic syenites represent the most radiogenic material associated with the Fogo A deposit.

Glass and sanidine strontium isotope compositions

Glass separates from six samples exhibit a range in $^{87}Sr/^{86}Sr$ ratios from 0·7048 to 0·7052 (Table 2), and, similar to the whole rocks, the $^{87}Sr/^{86}Sr$ ratios are inversely correlated with Sr concentrations. With the exception of the least radiogenic sample, the whole rocks are more radiogenic than the corresponding glass separate, and the overall range in $^{87}Sr/^{86}Sr$ ratios of the glasses is much smaller than that of the whole rocks (Fig. 4). The sanidine crystals exhibit a range in $^{87}Sr/^{86}Sr$ ratios both between and within samples, with the full range (0·7048–0·7062) found within a single sample (ASM-201) (Table 2). The most radiogenic sanidine has a higher $^{87}Sr/^{86}Sr$ ratio than the most radiogenic whole-rock trachytic pumice and glass separate, but is less radiogenic than the most radiogenic syenite. The Pb isotopic compositions of all of the sanidine crystals are indistinguishable from the whole-rock hosts.

Glass thorium and neodymium isotope compositions

Six glass separates exhibit a range in measured Th activity ratios, shown as ($^{230}Th/^{232}Th$), from 0·8724 to 0·8795. This variation is only slightly outside analytical uncertainty ($\pm 0{\cdot}0026$). However, the $(^{230}Th/^{232}Th)_o$ values corrected for eruption age (denoted by the subscript) range from 0·8737 to 0·8841 (Table 2) and are inversely correlated with Th concentrations, with the most evolved samples having the lowest $(^{230}Th/^{232}Th)_o$. The $(^{230}Th/^{232}Th)_o$ values were calculated based on the measured ($^{230}Th/^{238}U$) of each sample and an eruption age of 4600 years BP (Shotton *et al.*, 1969). The $(^{230}Th/^{232}Th)_o$ values of the Fogo A glasses are consistently lower than those reported for Azores basalts (0·89–1·4) (Turner *et al.*, 1997; Widom *et al.*, 1997; Claude-Ivanaj *et al.*, 2001). The $^{143}Nd/^{144}Nd$ ratios of the six glass separates do not vary outside analytical uncertainty. Although the averaged $^{143}Nd/^{144}Nd$ ratio of the six glasses (0·512767) is higher than the averaged $^{143}Nd/^{144}Nd$ ratio of the seven whole-rock pumices (0·512737), this difference is within our analytical uncertainty.

Leached trachytic glass strontium isotope compositions

Leaching experiments were performed to investigate the source of the high $^{87}Sr/^{86}Sr$ component(s) in the Fogo A trachytic pumices. Because of the Sr isotope heterogeneity

Table 1: Geochemical and isotopic data for whole-rock trachytic pumice and syenite samples from the Fogo A deposit, São Miguel, Azores

	Stratigraphic position (m)	Sr (ppm)	Rb (ppm)	Sm (ppm)	Nd (ppm)	Hf (ppm)	$^{87}Sr/^{86}Sr$	$^{87}Rb/^{86}Sr$	$^{143}Nd/^{144}Nd$	$^{176}Hf/^{177}Hf$	$^{206}Pb/^{204}Pb$	$^{207}Pb/^{204}Pb$	$^{208}Pb/^{204}Pb$
Whole-rock pumices													
ASM-218	4·78	478	152·4	10·2	73·5	16·9	0·704899	0·934	0·512732	0·282806	19·942	15·739	40·18
ASM-202	4·54	202	141·0	9·29	57·2	15·2	0·704977	2·04	0·512719	0·282804	19·915	15·735	40·10
ASM-201	2·53	41·4	167·4	11·3	70·3	19·8	0·705438	11·8	0·512743	0·282812	19·979	15·746	40·19
ASM-205	2·28	31·2	209·1	12·9	81·4	24·0	0·705043	19·6	0·512743	0·282813	19·950	15·742	40·19
ASM-210	1·51	3·40	254·9	16·1	102	27·0	0·706012	219	0·512740	0·282800	19·957	15·746	40·20
ASM-209a	1·36	32·5	297·1	19·1	138	—	0·705688	26·8	0·512736	—	19·944	15·738	40·17
ASM-224	0·59	6·39	270·9	17·6	113	—	0·706189	124	0·512744	—	19·968	15·760	40·24
Syenites													
T41		8					0·705531						
19#2		10					0·705339						
202s		41					0·705039						
6T1		31					0·704852						
T12		12					0·705011						
T21		14					0·704840						
T33		10					0·704993						
10		6					0·704858						
T32		6					0·704961						
T11		20					0·704871						
235s		7					0·705691						
207s		7					0·706974						

Whole-rock trachyte Sr, Rb, Nd, Sm and Hf concentrations determined by isotope dilution. Syenite Sr concentrations determined by X-ray fluorescence (Widom *et al.*, 1993).

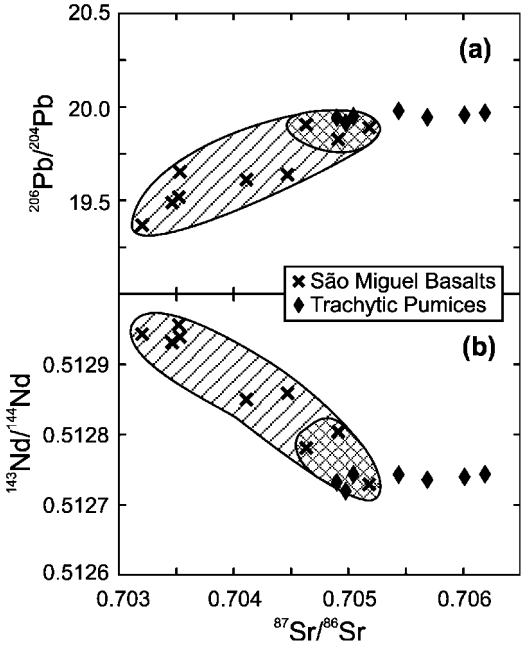

Fig. 3. Pb and Nd isotopic compositions of São Miguel basalts (diagonal stripes) and Fogo-flanking basalts (cross-hatched) and whole-rock Fogo A trachytes plotted vs $^{87}Sr/^{86}Sr$. (a) $^{206}Pb/^{204}Pb$ vs $^{87}Sr/^{86}Sr$. The highest $^{206}Pb/^{204}Pb$ ratios of the flanking basalts are the same as those for the Fogo A trachytes. (b) $^{143}Nd/^{144}Nd$ vs $^{87}Sr/^{86}Sr$. The lowest $^{143}Nd/^{144}Nd$ value of the flanking basalts is the same as that of the trachytes. The most radiogenic (Sr) basalts have similar $^{87}Sr/^{86}Sr$ ratios to the least radiogenic trachytes. Basalt data from Widom *et al.* (1997).

amongst the sanidine crystals within individual pumices, it was not possible to identify the source of the high $^{87}Sr/^{86}Sr$ component by leaching the whole-rock pumices in total. Therefore, the leaching experiments were conducted on two hand-picked glass separates including both the least radiogenic (ASM-218) and one of the most radiogenic (ASM-210) pumices. The hand-picked glasses were powdered by mortar and pestle. Four separate leaches were conducted on both samples: (1) 10 min in 5 ml high-purity water in an ultrasonic bath; (2) 10 min in 5 ml 1N HCl in an ultrasonic bath; (3) 10 min in 5 ml 4N HCl in an ultrasonic bath; (4) 15 min in 5 ml 4N HCl in an ultrasonic bath followed by addition of four drops of concentrated HF with continued sonication for 5 min. At the end of each leach step the leachate was removed and saved, and the samples were rinsed thoroughly with high-purity water, combining the rinse with the leachate. The leachates and final powder residue were then dried and spiked for isotope dilution analyses. The results are presented in Table 3 and Fig. 5. The percentage of Sr removed during each leach step is similar between both samples and ~77% of the total Sr remained in the powder residues. The leachable radiogenic Sr appears to have been removed by the end of the second leach (1N HCl), as the two subsequent leachates and the powder residues have the same $^{87}Sr/^{86}Sr$ ratios for each sample. The two powder residues retain slightly different final Sr isotopic compositions (ASM-210, 0·70504; ASM-218, 0·70493) from one another (Fig. 5) and are the same as those of the respective glass separates cleaned with 2N HCl (Table 2). Thus, the variations in $^{87}Sr/^{86}Sr$ in the evolved glass separates are not signatures of post-eruptive alteration, but rather indicate isotopic variability within the pre-eruptive magma chamber. These results also suggest that at least part of the radiogenic signature exhibited by the whole-rock trachytic pumices is due to post-magmatic surface contamination, as this easily leachable radiogenic Sr component must be present in the whole rocks.

DISCUSSION

The observed isotopic signatures in the glass separates and single sanidine crystals are a key to elucidating the magmatic processes that preceded the Fogo A eruption. Significant observations that need to be addressed include the following: the whole-rock trachytic pumice Nd, Pb and Hf isotopic compositions are constant throughout the deposit; the glass separates exhibit a small range in $^{87}Sr/^{86}Sr$ ratios that varies outside analytical error; the glass separates exhibit a narrow range in $(^{230}Th/^{232}Th)_o$; the sanidine phenocrysts exhibit a range in $^{87}Sr/^{86}Sr$ ratios both within and between samples, and many of these phenocrysts are more radiogenic than both the whole rock and glass from within a given sample. In the discussion that follows, we attempt to address all of these observations.

Pre- vs post-eruptive signatures

Several studies have identified post-magmatic alteration as a mechanism affecting the Sr isotopic compositions of evolved volcanic rocks (i.e. Halliday *et al.*, 1984; Cousens *et al.*, 1993; Kar *et al.*, 1998). Halliday *et al.* (1984) suggested post-eruptive alteration of glass by high $^{87}Sr/^{86}Sr$ groundwater or fluids as a mechanism for introducing Sr isotopic disequilibrium between glasses and feldspars in aged glassy pyroclastic rocks from the Bishop Tuff. Similarly, Kar *et al.* (1998) proposed that the high $^{87}Sr/^{86}Sr$ in the trachytic and rhyolite flows and pumice from Ascension is generated by subsolidus interaction of the felsic rocks with geothermal fluids. This interpretation is based on whole-rock and feldspar separate Sr isotopic data. The $^{87}Sr/^{86}Sr$ ratios of the feldspars are similar to those of the mafic rocks on the island, and acid leaching of the whole rocks removed their radiogenic signature (Kar *et al.*, 1998). As demonstrated in the leaching experiments of silicic ignimbrites by Cousens *et al.* (1993), Rb and Sr can be mobilized during subsolidus processes while leaving

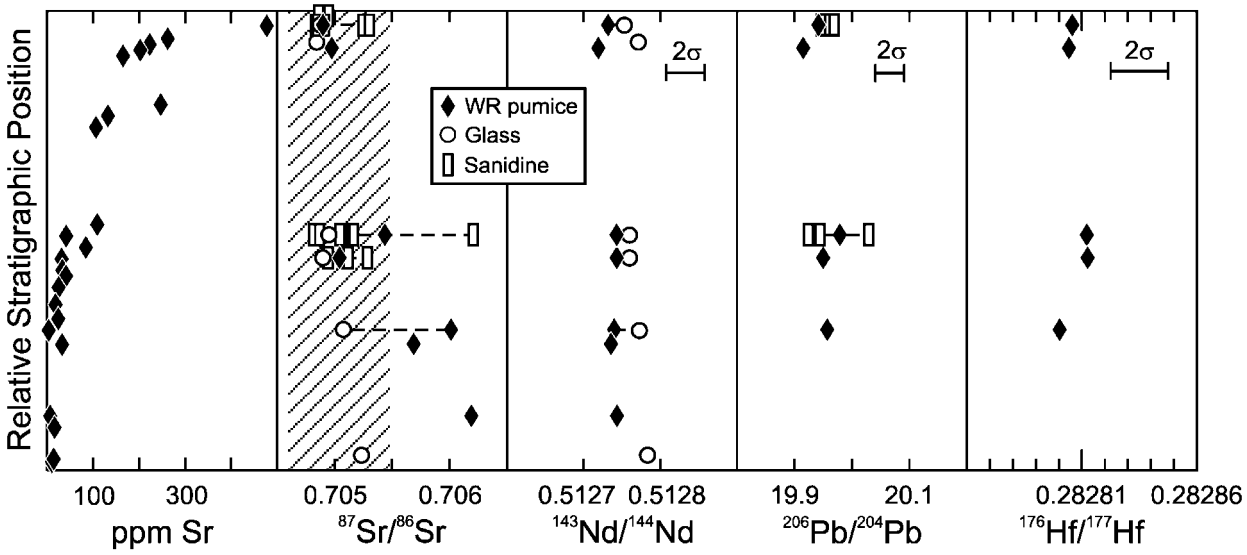

Fig. 4. Relative stratigraphic position vs Sr concentration and isotopic composition of whole-rock trachytic pumices (◆) trachytic glasses (○) and individual sanidine crystals (open rectangles). Sr, behaving compatibly as a result of feldspar fractionation, shows a significant increase in concentration from the bottom to top of the sampled Fogo A deposit [data from Widom *et al.* (1992)]. The Sr isotope ratios correlate with stratigraphic position in the deposit, and are inversely correlated with Sr concentration (2σ errors are smaller than the symbols). The range in $^{87}Sr/^{86}Sr$ ratios is smaller for the glasses than it is for the whole rocks, but the Sr isotopic compositions of the glasses vary outside 2σ error. The diagonally shaded region represents the range in $^{87}Sr/^{86}Sr$ ratios exhibited by the basalts flanking the Fogo volcano. The $^{143}Nd/^{144}Nd$, $^{206}Pb/^{204}Pb$ and $^{176}Hf/^{177}Hf$ ratios of the whole rocks are constant within 2σ error throughout the deposit. The $^{143}Nd/^{144}Nd$ ratios of the whole rocks and glasses do not differ from one another outside analytical uncertainty. Whole rocks and corresponding glass separates and sanidine crystals are connected with dashed lines where symbols do not overlap.

Nd and Pb isotope ratios undisturbed. Alteration of the $^{87}Sr/^{86}Sr$ ratios will be stronger in highly evolved rocks with low Sr concentrations.

In the Fogo A deposit, surface accumulation of salts derived from sea spray ($^{87}Sr/^{86}Sr = 0{\cdot}709$) probably contributes to the leachable radiogenic Sr signature of the glass separates, but must be combined with an additional easily leachable source of Sr (possibly from meteoric water) to explain our leaching results (leachate $^{87}Sr/^{86}Sr \leq 0{\cdot}7059$). Despite the fact that low-Sr glass separates from Fogo A exhibit the highest $^{87}Sr/^{86}Sr$ ratios, there is no evidence in our leaching data to suggest that the observed range in $^{87}Sr/^{86}Sr$ ratios of the glass is due to post-eruptive alteration. The glass separates were cleaned with 2N HCl for 10 min, whereas results of our leaching experiments indicate that a 10 min leach in 1N HCl adequately removed all leachable radiogenic Sr. We have demonstrated that extensive post-eruptive alteration cannot explain the Sr isotope variations in the Fogo A glass separates. Therefore, we now consider possible pre-eruptive mechanisms to explain the observed Sr and Th isotope variations, including both closed-system and open-system processes.

Closed- vs open-system processes

Closed-system processes

Simple closed-system crystal fractionation does not appear to be a viable explanation for the Sr isotopic compositions of the Fogo A trachytic glasses. Although the glass separates exhibit a positive slope on a Rb–Sr isochron diagram, they do not display an isochronous relationship ($r^2 < 0{\cdot}81$). In addition, within a given sample, the sanidine phenocrysts have $^{87}Sr/^{86}Sr$ similar to or higher than the whole rocks and glass, yet have Rb/Sr either similar to (ASM-218) or lower than (ASM-201 and 205) the host glass. Consequently, the radiogenic $^{87}Sr/^{86}Sr$ ratios of the sanidines compared with the glasses cannot be the result of radiogenic ingrowth. The negative correlation of $(^{230}Th/^{232}Th)_o$ with $(^{238}U/^{232}Th)$ in the glass separates is also inconsistent with closed-system crystal fractionation; radiogenic ingrowth of ^{230}Th following closed-system crystal fractionation would result in the opposite correlation.

Open-system processes

Sr isotope data on phenocrysts and glass separates can provide important information regarding the relative timing of open-system processes. Isotopic disequilibrium between phenocrysts and more radiogenic host glass is indicative of assimilation or contamination of the magma subsequent to phenocryst formation, whereas glass and phenocrysts with similar isotopic compositions (in an isotopically zoned tephra) indicate that contamination of the magma occurred prior to the growth of the phenocrysts. Sr isotope disequilibrium between phenocrysts and

Table 2: Geochemical data for whole-rock trachytic pumice, glass and sanidine samples from the Fogo A deposit, São Miguel, Azores

Sample	Sr (ppm)	$^{87}Sr/^{86}Sr$	Rb (ppm)	$^{87}Rb/^{86}Sr$	Nd (ppm)	$^{143}Nd/^{144}Nd$	Pb (ppm)	$^{206}Pb/^{204}Pb$	$^{207}Pb/^{204}Pb$	$^{208}Pb/^{204}Pb$	Th (ppm)	$(^{230}Th/^{232}Th)_o$	$(^{234}U/^{238}U)$	$(^{238}U/^{232}Th)$
ASM-217 S1	374	0·704862												
ASM-217 S2	546	0·704947												
ASM-218 WR	478	0·704899	152	0·934	73·5	0·512732		19·942	15·739	40·18				
ASM-218 GL	57·6	0·704895	153	13·3	69·3	0·512756					20·72	0·8804	0·9999	0·8339
		0·704937												
ASM-218 S1	152	0·704910	69·8	1·34			5							
ASM-218 S2	166	0·704831	72·2	1·28			5							
ASM-218 S3	267	0·704848	4·99	0·182			4							
ASM-218 S4								19·961	15·747	40·20				
ASM-218 S5	164	0·705303	71·1	1·27				19·969	15·753	40·22				
ASM-218 S6	113	0·705246	68·5	1·77				19·946	15·742	40·18				
ASM-204 GL	179	0·704841	143	3·91	60·9	0·512773					18·03	0·8841	1·0005	0·7723
		0·704808												
ASM-201 WR	41·4	0·705438	167	11·8	70·3	0·512743		19·979	15·746	40·19				
ASM-201 GL	45·2	0·704948	162	21·3	73·8	0·512760					23·25	0·8782	1·0015	0·8200
		0·704963												
ASM-201 S1							3							
ASM-201 S2	227	0·704870	71·0	0·917			5							
ASM-201 S3	114	0·705045	132	3·40			5							
ASM-201 S4	10·9	0·705136	132	35·6				19·944	15·740	40·18				
ASM-201 S5								20·029	15·767	40·35				
ASM-201 S6								19·924	15·725	40·13				
ASM-201 S7	103	0·706208	75·7	2·14										
ASM-201 S8	68·3	0·705150	100	4·31										
ASM-201 S9	114	0·705166	98·8	2·54										
ASM-201 S10	132	0·704816	52·8	1·17										
ASM-205 WR	31·2	0·705043	209	19·6	81·4	0·512743								
ASM-205 GL	22·6	0·704895	216	57·2	83·9	0·512760					29·38	0·8780	1·0020	0·8047
		0·704895												

Table 2: continued

Sample	Sr (ppm)	$^{87}Sr/^{86}Sr$	Rb (ppm)	$^{87}Rb/^{86}Sr$	Nd (ppm)	$^{143}Nd/^{144}Nd$	Pb (ppm)	$^{206}Pb/^{204}Pb$	$^{207}Pb/^{204}Pb$	$^{208}Pb/^{204}Pb$	Th (ppm)	$(^{230}Th/^{232}Th)_o$	$(^{234}U/^{238}U)$	$(^{238}U/^{232}Th)$
ASM-205 S1	91·5	0·704943	85·3	2·73			5							
ASM-205 S2	37·2	0·705284	91·6	7·20			2							
ASM-205 S3	94·2	0·705118	58·1	1·80										
ASM-205 S4	52·0	0·705076	94·4	5·32										
ASM-210 WR	3·40	0·706012	255	219	102	0·512740								
ASM-210 GL	1·69	0·705071	260	1810	109	0·512767					41·20	0·8759	1·0022	0·8239
		0·705038												
ASM-220 GL	0·950	0·705214	387	1190	135	0·512785					67·65	0·8737	0·9995	0·8433

Sr, Rb, Nd, Pb and Th concentrations were determined by isotope dilution. Replicate analyses of $^{87}Sr/^{86}Sr$ ratios on five glass separates are shown in italics. Th isotopic compositions are reported as eruption age (4600 years BP) corrected activity ratios using the $(^{230}Th/^{238}U)$ ratios of the samples. Samples are arranged according to their relative stratigraphic position. WR, whole pumice; GL, glass; S, sanidine.

Table 3: Results of powdered trachytic glass leaching experiments for Sr isotope composition and Sr concentration by isotope dilution

	Sr (ng)	% of total Sr	$^{87}Sr/^{86}Sr$
ASM-210 GMQ	45·7	4·6	0·705912
ASM-210 GL1	94·9	9·5	0·705891
ASM-210 GL2	46·6	4·7	0·705037
ASM-210 GL3	52·3	5·2	0·705044
ASM-210 GLR	762	76·1	0·705030
Total	1000	100	
ASM-210 'cleaned'	964		0·705054
ASM-218 GMQ	180	3·8	0·705234
ASM-218 GL1	623	13·2	0·705055
ASM-218 GL2	85·4	1·8	0·704932
ASM-218 GL3	127	2·7	0·704933
ASM-218 GLR	3690	78·4	0·704938
Total	4700	100	
ASM-218 'cleaned'	4770		0·704916

GMQ, high-purity water leachate; GL1, 1N HCl leachate; GL2, 4N HCl leachate; GL3, 4N HCl + concentrated HF leachate; GLR, powder residue; 'cleaned' Sr values are expected total ng Sr based on amount of sample used and measured Sr concentration of sample cleaned with 2N HCl (Table 2), and 'cleaned' $^{87}Sr/^{86}Sr$ ratios are the average of the two replicate analyses for each sample (using the 2N HCl glass cleaning procedure described in the text) reported in Table 2.

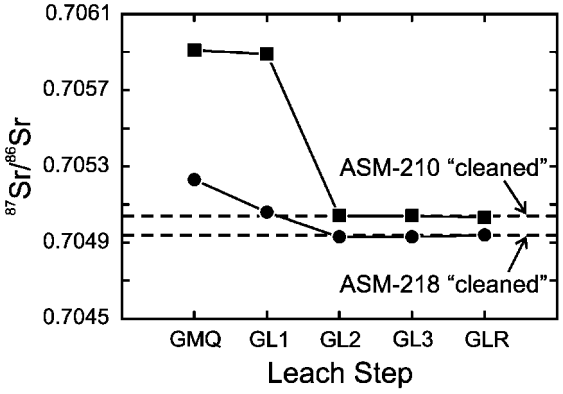

Fig. 5. $^{87}Sr/^{86}Sr$ vs leach step for glass separates ASM-210 (1·7 ppm Sr) and ASM-218 (57·6 ppm Sr). All radiogenic Sr was removed by the end of the second leaching step for both samples, suggesting that $^{87}Sr/^{86}Sr$ ratios reported for the glass separates in Table 2 represent magmatic compositions. GMQ, 10 min leach in high-purity water; GL1, 10 min leach in 1N HCl; GL2, 10 min leach in 4N HCl; GL3, 15 min leach in 4N HCl + 5 min with four drops of concentrated HF; GLR, powder residue after step GL3.

matrix has been identified in numerous cases in continental and oceanic settings, but in all of these cases, the Sr isotopic composition of glass is more radiogenic than the phenocrysts (Halliday *et al.*, 1984; Wörner *et al.*, 1985; Palacz & Wolff, 1989; Kar *et al.*, 1998).

Sr isotopic disequilibrium between Fogo A glasses and sanidines. Our data indicate significant isotopic disequilibrium between phenocrysts and glass in the Fogo A trachyte deposit, based on the analysis of individual sanidine crystals and unaltered glasses. However, unlike the cases of the Bishop Tuff, Laacher See and Grandilla pumice cited previously, the glass in the Fogo A trachyte has $^{87}Sr/^{86}Sr$ either the same as or lower than the sanidine phenocrysts.

One possible mechanism causing the high $^{87}Sr/^{86}Sr$ ratios in some of the sanidines could be *in situ* radioactive ingrowth of ^{87}Sr, by which crystals initially in radioactive equilibrium with the liquid become more radiogenic as a function of their residence times in the magma chamber and their Rb/Sr ratios. The maximum amount of time over which this could occur can be assumed to be 200 kyr, based on the age of the oldest dated material associated with the Fogo volcano. Sr diffusion in sanidine at magmatic temperatures should have a negligible effect on the $^{87}Sr/^{86}Sr$ ratios of these crystals over 200 kyr, based on the low diffusion rates reported by Cherniak (1996). Using 200 kyr as the maximum allowable time, the measured $^{87}Rb/^{86}Sr$ ratios for each of the sanidines, and the $^{87}Sr/^{86}Sr$ ratio of the respective glass separates, the maximum $^{87}Sr/^{86}Sr$ ratios attainable by *in situ* radioactive decay were calculated (0·704896–0·705049). Because the measured $^{87}Sr/^{86}Sr$ ratios of many of the sanidines (up to 0·706208) are far higher than the calculated maximum $^{87}Sr/^{86}Sr$ ratios that could result from *in situ* radioactive ingrowth over the life span of the Fogo volcano, the Sr isotope compositions of the sanidine crystals cannot easily be explained by this mechanism alone.

A potential source of radiogenic Sr for the sanidines is syenite within the volcano's intrusive complex, as sampled in the form of xenolithic syenite nodules within the Fogo A deposit. Although the least radiogenic syenite in the Fogo A deposit has the same Sr isotopic composition as the least radiogenic Fogo A glass and sanidine ($^{87}Sr/^{86}Sr = 0{\cdot}70484$), and is interpreted to represent the uncontaminated pre-eruptive Fogo A Sr isotope composition, other syenites range in $^{87}Sr/^{86}Sr$ up to 0·70697. The existence of quartz with highly saline (salt crystal-bearing) fluid inclusions has been interpreted as evidence for interaction of the syenites with high-salinity, aqueous fluids (Widom *et al.*, 1993; E. Widom, unpublished data, 1990). Although Larson *et al.* (2001) have shown that meteoric water can dominate hydrothermal fluids in an ocean island setting, the hydrothermal system in an ocean

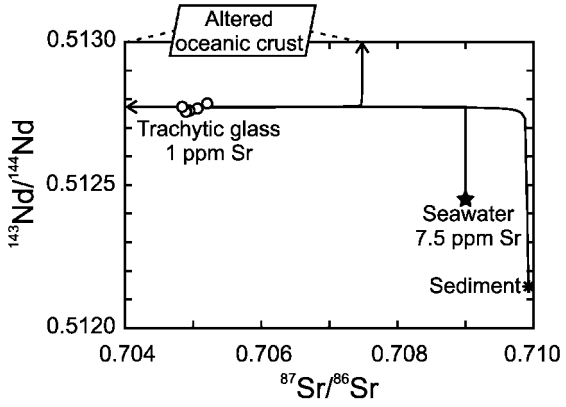

Fig. 6. Mixing curves on a $^{143}Nd/^{144}Nd$ vs $^{87}Sr/^{86}Sr$ diagram illustrating models for producing radiogenic Sr in Fogo A trachytic glasses. Although the glasses exhibit a range in $^{87}Sr/^{86}Sr$ ratios their $^{143}Nd/^{144}Nd$ isotope ratios are indistinguishable from one another. This diagram illustrates calculated mixing paths between the least radiogenic trachytic glass and (1) seawater (star), (2) Atlantic Ocean sediments (asterisk) (Ben Othman *et al.*, 1989), and (3) altered oceanic crust (Staudigel *et al.*, 1995). The dashed lines indicate the potential range in $^{87}Sr/^{86}Sr$ of altered oceanic crust. Essentially identical mixing curves are generated on plots of $^{176}Hf/^{177}Hf$ and $^{206,207,208}Pb/^{204}Pb$ vs $^{87}Sr/^{86}Sr$.

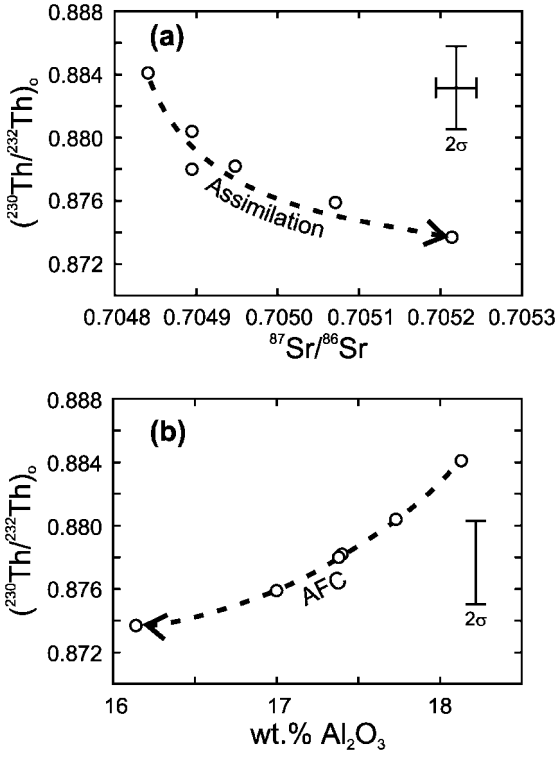

Fig. 7. (a) The $(^{230}Th/^{232}Th)_o$ and $^{87}Sr/^{86}Sr$ of the Fogo A glass separates are inversely correlated, suggestive of assimilation of material possessing low $(^{230}Th/^{232}Th)_o$ and high $^{87}Sr/^{86}Sr$ relative to the most evolved trachytic glass. (b) $(^{230}Th/^{232}Th)_o$ vs wt % Al_2O_3 where Al_2O_3 decreases with increasing sanidine fractionation. The correlations of $(^{230}Th/^{232}Th)_o$ with $^{87}Sr/^{86}Sr$ and Al_2O_3 are suggestive of AFC processes involving a contaminant characterized by low $(^{230}Th/^{232}Th)_o$ and high $^{87}Sr/^{86}Sr$ relative to the most evolved trachytic glass (lowest Al_2O_3). Al_2O_3 data from Widom *et al.* (1992). Error bars represent 2σ analytical uncertainty.

island setting may represent a mixture of seawater and meteoric fluids (Kar *et al.*, 1998), which would provide a potential source of radiogenic Sr.

Incorporation of high $^{87}Sr/^{86}Sr$ sanidine crystals (up to 200 ppm Sr) from radiogenic, hydrothermally altered syenite similar to those observed (or similar older plutonic rock) by relatively low Sr Fogo A liquid (1–2 ppm Sr) could account for the elevated Sr isotopic compositions of some of the whole-rock trachytic pumices. For example, one sanidine of typical size (20 mg) incorporated as a xenocryst from syenite 207 s ($^{87}Sr/^{86}Sr = 0{\cdot}70697$) into 2 g of glass (liquid) with $^{87}Sr/^{86}Sr = 0{\cdot}7051$ could raise the $^{87}Sr/^{86}Sr$ ratio of the whole rock to 0·706.

Isotopic variation in trachytic glasses. Although the range in Sr isotopic composition of the trachytic glass (0·7048–0·7052) is much smaller than the range exhibited by the whole-rock trachytic pumices (0·7049–0·7062), the range in Sr isotopic compositions of the glasses is significantly outside analytical error. Potential sources for radiogenic Sr in a young (<200 ka) ocean island setting are limited owing to the lack of radiogenic continental crust. However, seawater, marine sediments, altered oceanic crust and aged and/or hydrothermally altered rocks (including syenites) making up the volcanic edifice are possible candidates.

Sr, Nd, Pb and Hf isotopic data do not allow the potential contaminants to be uniquely identified (Fig. 6). Mixing paths were calculated assuming that the range in Sr concentration of the glasses was present prior to the contamination event, and using the least radiogenic $^{87}Sr/^{86}Sr$ ratio of the glasses. Although these models allow for constraints to be placed on the amount of contamination involved, the mixing paths of altered oceanic crust, seawater and marine sediments are indistinguishable in the range of interest (Fig. 6).

The range in $(^{230}Th/^{232}Th)_o$ exhibited by the trachytic glass separates (0·8737–0·8841) cannot be explained by contamination of the Fogo A magma chamber by seawater, hydrothermally altered mid-ocean ridge basalt (MORB), or hydrothermally altered basalt from the volcanic edifice. Unreasonably large amounts of seawater are required to modify the $(^{230}Th/^{232}Th)_o$ of the Fogo A magma because seawater Th concentrations are extremely low ($\sim 9 \times 10^{-6}$ ppm) (Emsley, 1998).

Constraints on assimilation of other contaminants may be made based on the correlation of $(^{230}Th/^{232}Th)_o$ with $^{87}Sr/^{86}Sr$ and elemental concentrations. The inverse correlation of $(^{230}Th/^{232}Th)_o$ with $^{87}Sr/^{86}Sr$ is suggestive of assimilation resulting in a decrease in $(^{230}Th/^{232}Th)_o$ and a corresponding increase in $^{87}Sr/^{86}Sr$ (Fig. 7a). Both $(^{230}Th/^{232}Th)_o$ and $^{87}Sr/^{86}Sr$ also correlate well with

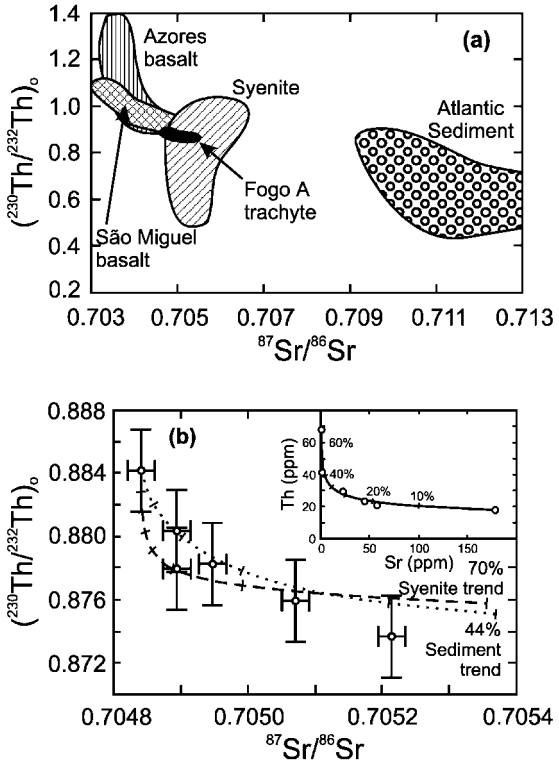

Fig. 8. (a) The (^{230}Th/^{232}Th) and ^{87}Sr/^{86}Sr compositions of potential contaminants relative to the Fogo A trachytic glasses (small black field). Suitable contaminants must have lower (^{230}Th/^{232}Th) than the most evolved Fogo A trachytic pumice, and are therefore limited to syenite wall rock and Atlantic Ocean sediments. Oceanic sediment data are from Ben Othman *et al.* (1989) and McDermott & Hawkesworth (1991), basalt data from Turner *et al.* (1997), Widom *et al.* (1997) and Claude-Ivanaj *et al.* (2001), and syenite data from this study and Widom *et al.* (1993). (b) AFC models with syenite wall rock (dashed line) and marine sediment (dotted line) as the assimilants. Tick marks represent per cent crystallization. Approximately 69% crystallization is required to account for the observed Th and Sr concentration (inset) and isotopic variation in the Fogo A trachytic glasses. The continuous line in the inset is the AFC path for both syenite and sediment. The tick marks in the inset represent per cent crystallization using syenite as the assimilant. Assimilation of sediment results in slightly lower Th/Sr ratios for given percentage of crystallization. Input parameters: least evolved, uncontaminated Fogo A magma—18·03 ppm Th, 178·5 ppm Sr, ^{87}Sr/^{86}Sr = 0·70484, (^{230}Th/^{232}Th) = 0·8841; contaminating syenite—40 ppm Th, 10 ppm Sr, ^{87}Sr/^{86}Sr = 0·70620, (^{230}Th/^{232}Th) = 0·8100; $D_{Sr} = 6$; $D_{Th} = 0·001$; $r = 0·075$; contaminating sediment—10 ppm Th, 70 ppm Sr, ^{87}Sr/^{86}Sr = 0·709, (^{230}Th/^{232}Th) = 0·45; $D_{Sr} = 6$; $D_{Th} = 0·001$; $r = 0·08$.

major elements. The correlation of $(^{230}Th/^{232}Th)_o$ with Al_2O_3 is consistent with assimilation–fractional crystallization (AFC) processes in which fractional crystallization of sanidine causes a decrease in Al_2O_3 and assimilation is responsible for the decrease in $(^{230}Th/^{232}Th)_o$ (Fig. 7b).

Crustal lithologies characterized by low $(^{230}Th/^{232}Th)_o$ and high $^{87}Sr/^{86}Sr$, relative to the most evolved trachytic glass, must be evaluated as potential contaminants. The (^{238}U/^{232}Th) ratios of altered oceanic crust can range from 1·7 to >20 (Staudigel *et al.*, 1995). Old altered oceanic crust (in radioactive equilibrium) thus should have (^{230}Th/^{232}Th) >1·7, significantly higher than that required of the Fogo A contaminant, which must be <0·8737. Thus, altered MORB cannot be considered a likely contaminant of the Fogo magma chamber. The (^{238}U/^{232}Th) values of some young basalts from the Azores (0·797–1·13) are similar to those measured on the trachytic glasses (Turner *et al.*, 1997; Widom *et al.*, 1997; Claude-Ivanaj *et al.*, 2001), and thus with aging and growth towards radioactive equilibrium could develop (^{230}Th/^{232}Th) sufficiently low to be considered as potential contaminants. However, older submarine Fogo basalts would be expected to experience U enrichment during seawater alteration; thus they also would be expected to have (^{230}Th/^{232}Th) higher than that of the Fogo A contaminant. Subaerially altered edifice basalts may have experienced preferential U loss similar to subaerially altered basalts at Mauna Loa (Cohen *et al.*, 1996). Assimilation of such material by the Fogo A magma could produce the observed decrease in (^{230}Th/^{232}Th), but should not result in the observed increase in ^{87}Sr/^{86}Sr ratios, as subaerial alteration is unlikely to produce substantially elevated ^{87}Sr/^{86}Sr ratios in basalts.

The (^{230}Th/^{232}Th) of aged wall rock syenite (0·5–1) (Widom *et al.*, 1993) and marine sediments (0·3–1·3) (Ben Othman *et al.*, 1989; McDermott & Hawkesworth, 1991) are sufficiently low to cause a decrease in the (^{230}Th/^{232}Th) of the Fogo A magma via contamination (Fig. 8a). Calculated AFC models (DePaolo, 1981) indicate that the observed variations in the Sr and Th concentrations in the Fogo A glasses could be produced by ~70% crystallization combined with a moderate assimilation rate (r = 0·075) of either marine sediment or syenite wall rock (Fig. 8b, inset). However, combined fractional crystallization and assimilation of marine sediment produces rapid changes in the Sr isotopic signature (Fig. 8b), and cannot simultaneously account for both the observed Sr and Th concentration and isotopic variations. Unreasonably high (>1) Th/Sr ratios in the assimilating sediment over a wide range of assimilation rates (r = 0·02–0·1) would be required to reproduce the trachytic glass data. In contrast, the observed Sr and Th concentration and isotopic variations can be achieved via ~69% crystallization combined with ~5% bulk assimilation of the syenite wall rock (r = 0·075) (Fig. 8b). Although the temperature of the syenite is poorly constrained, these data can be reproduced using the energy-constrained AFC model of Spera & Bohrson (2001).

Additional constraints on assimilation may be made based on $\delta^{18}O$ from two glass separates ($\delta^{18}O$ = 6·2 and 6·3 ± 0·30‰ for ASM-204 and ASM-210, respectively), which indicate that there is no variation in $\delta^{18}O$ despite significant differences in $(^{230}Th/^{232}Th)_o$ and $^{87}Sr/^{86}Sr$ (0·7048 and 0·7051). The measured oxygen

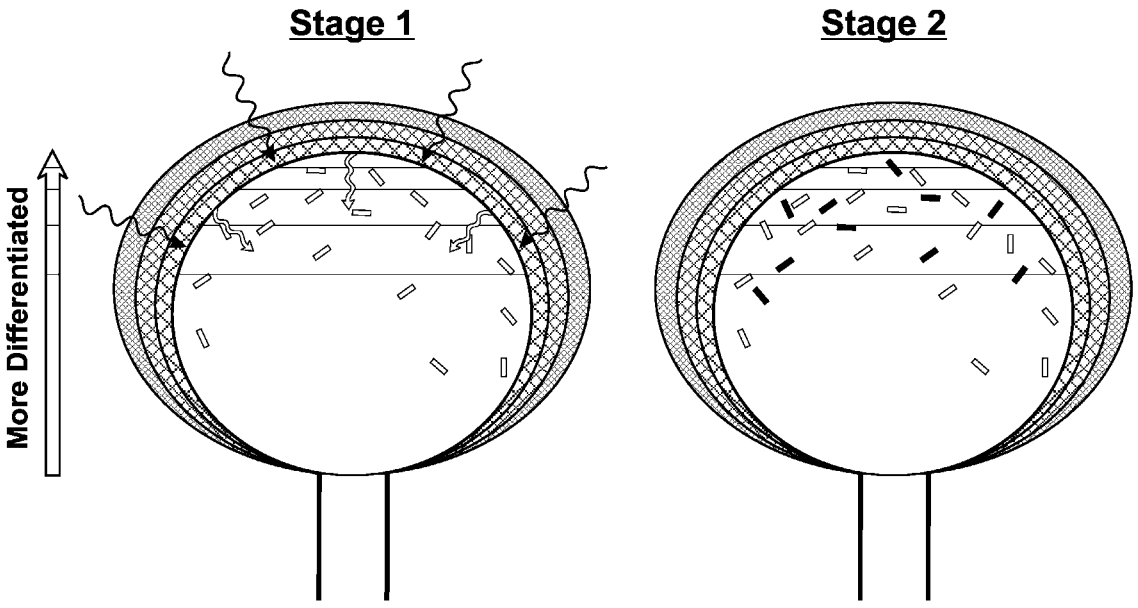

Fig. 9. A schematic representation of the Fogo A magma chamber illustrating the two distinct stages of contamination. Stage 1 involves variable hydrothermal fluid modification of the syenite wall rock (black arrows) (Widom *et al.*, 1993). During this stage the Sr isotopic composition of the wall rock is elevated as high as 0·70697, and fractional crystallization and assimilation of syenite melts occur (white arrows), resulting in the development of chemical and isotopic (Sr and Th) zonation within the pre-eruptive magma chamber. Stage 2 (prior to or during eruption) involves incorporation of xenocrystic sanidines (illustrated as black crystals) from the fluid-modified wall rock. The small but significant range in the Sr and Th isotopic compositions of the glass separates, and the elevated $^{87}Sr/^{86}Sr$ ratios in some of the sanidine phenocrysts require these two distinct contamination methods.

isotopic compositions of the glasses are an upper limit for the $\delta^{18}O$ of the magma, because post-eruptive exchange will result in elevated $\delta^{18}O$ even in petrographically pristine glass (Muehlenbachs, 1987; Cousens *et al.*, 1993). However, even 5% assimilation of sediment should result in elevation of $\delta^{18}O$ of the more evolved trachytic pumices to at least 7·0‰, owing to the high $\delta^{18}O$ of marine sediments (15–25‰) (Eiler *et al.*, 1997). Sediment assimilation thus cannot explain the radiogenic Sr and low $(^{230}Th/^{232}Th)_o$ of the evolved glasses. In contrast, 5% assimilation of syenite would not significantly affect the magmatic $\delta^{18}O$, based on preliminary $\delta^{18}O$ in Fogo syenites (2·6 to 5·6 ± 0·30‰). These results therefore also suggest that syenite, rather than marine sediment, is probably responsible for the observed Sr and Th isotope variations.

Multi-stage open-system evolution model

We propose that three processes are responsible for the Sr isotope variations observed within the Fogo A trachytic pumice deposit. Two magmatic processes are proposed to explain the variations in Sr and Th isotopic compositions of the glasses and the radiogenic signature exhibited by the sanidines. These two processes are divided into Stage 1 and Stage 2 (Fig. 9). Stage 1 involves hydrothermal alteration by seawater-derived fluids of the syenite wall rock and contamination of the Fogo A magma by melts from this altered rock. Hydrothermal alteration of the wall rock results in elevated $^{87}Sr/^{86}Sr$ ratios ($\geq$0·707) while leaving the $(^{230}Th/^{232}Th)$ unchanged. Assimilation of the wall rock is required to explain the Sr and Th isotope variability in the glass. Although the syenitic wall rock is thought to be the plutonic equivalent of the pre-eruptive Fogo A magma and older trachytic liquids, we suggest that the Fogo A magma chamber experienced a complex thermal history, which caused remelting of the syenites. Multiple episodes of basaltic volcanism occurred on the flanks of the Fogo volcano prior to the Fogo A eruption, providing a heat source for remelting and assimilation of the syenite wall rock into the Fogo A magma. This contamination is envisioned to have occurred concurrent with the development of the chemical zonation via crystal fractionation within the magma chamber. Stage 2 involves incorporation of xenocrystic sanidines from the previously altered wall rock, probably during the eruption, and accounts for the variable and highly radiogenic sanidine Sr isotopic compositions. The origin of the radiogenic sanidines described here may be analogous to those from the Bandelier Tuff described by Wolff *et al.* (2002). The third process is post-eruptive surface alteration, which results in the elevation of the whole-rock and glass $^{87}Sr/^{86}Sr$ ratios, without affecting phenocrysts.

CONCLUSION

Whole-rock trachytic pumices show variation in Sr and Th isotopic compositions that can be attributed to melting and assimilation of hydrothermally altered wall rock, incorporation of radiogenic xenocrystic sanidine from the syenite wall rock, and post-eruptive alteration. Sr and Th isotopic compositions of the trachytic glasses are controlled by contamination of the magma by hydrothermally altered wall rock that had low ($^{230}Th/^{232}Th$) as a result of aging and whose Sr isotopic compositions have been influenced by seawater. The compositionally variable and radiogenic sanidines are explained by incorporation of xenocrystic sanidine from disaggregation of hydrothermally altered (high $^{87}Sr/^{86}Sr$) syenitic wall rock. Because of the low $Sr_{glass}/Sr_{sanidine}$ ratios, only one or two crystals of radiogenic sanidine (150–300 μg each) per 2–4 g of glass would elevate the $^{87}Sr/^{86}Sr$ ratios of the whole rocks.

Our results emphasize that magmatic systems whose chemical variations appear fully consistent with closed-system processes (e.g. Widom *et al.*, 1993) may nevertheless have experienced complex open-system processes. Our results also emphasize that isotopic analyses of whole rocks can be misleading if interpreted as 'liquid' compositions. To gain a detailed understanding of petrogenetic processes, it is critical to obtain isotopic data on glass and mineral separates. Our results also highlight the fact that multiple open-system processes may operate in a given magmatic system, and different processes may be recorded in mineral vs glass compositions.

ACKNOWLEDGEMENTS

M. Horan and T. Mock are thanked for assistance with all isotope analyses at the Department of Terrestrial Magnetism. Mark Reagan, John Wolff and Dennis Geist provided thorough and insightful comments on an earlier draft. Financial support for this project was provided by the Geological Society of America (student research awards to D.S. 2000 and 2001), Sigma Xi (Grants-in-Aid of research awards to D.S. 2000 and 2001) and the National Science Foundation (NSF EAR 0207529 and EAR 9902956 awarded to E.W.)

REFERENCES

Ben Othman, D., White, W. M. & Patchett, J. (1989). The geochemistry of marine sediments, island arc magma genesis, and crust–mantle recycling. *Earth and Planetary Science Letters* **94**, 1–21.

Bindeman, I. N. & Valley, J. W. (2001). Low-$\delta^{18}O$ rhyolites from Yellowstone: magmatic evolution based on analyses of zircons and individual phenocrysts. *Journal of Petrology* **42**, 1491–1517.

Blake, S. (1984). Volatile oversaturation during the evolution of silicic magma chambers as an eruption trigger. *Journal of Geophysical Research* **89**, 8237–8244.

Blichert-Toft, J., Chauvel, C. & Albarède, F. (1997). Separation of Hf and Lu for high-precision isotope analysis of rock samples by magnetic sector-multiple collector ICP-MS. *Contributions to Mineralogy and Petrology* **127**, 248–260.

Booth, B., Croasdale, R. & Walker, G. (1978). A quantitative study of five thousand years of volcanism on São Miguel, Azores. *Philosophical Transactions of the Royal Society of London* **288**, 271–319.

Bursik, M. I., Sparks, R. S. J., Gilbert, J. S. & Carey, S. N. (1992). Sedimentation of tephra by volcanic plumes: I. Theory and its comparison with a study of the Fogo A plinian deposit, São Miguel (Azores). *Bulletin of Volcanology* **54**, 329–344.

Cameron, K. L. & Cameron, M. (1986). Whole-rock/groundmass differentiation trends of rare earth elements in high-silica rhyolites. *Geochimica et Cosmochimica Acta* **50**, 759–769.

Cherniak, D. J. (1996). Strontium diffusion in sanidine and albite, and general comments on strontium diffusion in alkali feldspars. *Geochimica et Cosmochimica Acta* **60**, 5037–5043.

Christensen, J. N. & DePaolo, D. J. (1993). Timescales of large volume silicic magma systems: Sr isotopic systematics of phenocrysts and glass from the Bishop Tuff, Long Valley, California. *Contributions to Mineralogy and Petrology* **113**, 100–114.

Claude-Ivanaj, C., Jouron, J.-L. & Allègre, C. J. (2001). ^{238}U–^{230}Th–^{226}Ra fractionation in historical lavas from the Azores: long-lived source heterogeneity vs metasomatism fingerprints. *Chemical Geology* **176**, 295–310.

Cohen, A. S., O'Nions, R. K. & Kurz, M. D. (1996). Chemical and isotopic variations in Mauna Loa tholeiites. *Earth and Planetary Science Letters* **143**, 111–124.

Cousens, B. L., Spera, F. J. & Dobson, P. F. (1993). Post-eruptive alteration of silicic ignimbrite lavas, Gran Canaria, Canary Islands: strontium, neodymium, lead, and oxygen isotopic evidence. *Geochimica et Cosmochimica Acta* **57**, 631–640.

Deniel, C. & Pin, C. (2001). Single-stage method for the simultaneous isolation of lead and strontium from silicate samples for isotopic measurements. *Analytica Chimica Acta* **426**, 95–103.

DePaolo, D. J. (1981). Trace element and isotopic effects of combined wallrock assimilation and fractional crystallization. *Earth and Planetary Science Letters* **53**, 189–202.

Eichelberger, J. C., Chertkoff, D. G., Dreher, S. T. & Nye, C. J. (2000). Magmas in collision: rethinking chemical zonation in silicic magmas. *Geology* **28**, 603–606.

Eiler, J. M., Farley, K. A., Valley, J. W., Hauri, E., Craig, H., Hart, S. R. & Stolper, E. M. (1997). Oxygen isotope variations in ocean island basalts. *Geochimica et Cosmochimica Acta* **61**, 2281–2293.

Emsley, J. (1998). *The Elements*, 3rd edn. New York: Oxford University Press.

Gandino, A., Guidi, M., Merlo, C., Mete, L., Rossi, R. & Zan, L. (1985). Preliminary model of the Ribeira Grande geothermal field (Azores Islands). *Geothermics* **14**, 91–105.

Halliday, A. N., Fallick, A. E., Hutchinson, J. & Hildreth, W. (1984). A Nd, Sr, and O isotopic investigation into the causes of chemical and isotopic zonation in the Bishop Tuff, California. *Earth and Planetary Science Letters* **68**, 379–391.

Hildreth, W. (1981). Gradients in silicic magma chambers: implications for lithospheric magmatism. *Journal of Geophysical Research* **86**, 10153–10192.

Hildreth, W., Christiansen, R. L. & O'Neil, J. R. (1984). Catastrophic isotopic modification of rhyolitic magma at times of caldera subsidence, Yellowstone Plateau Volcanic Field. *Journal of Geophysical Research* **89**, 8339–8369.

Johnson, C. M. (1989). Isotopic zonations in silicic magma chambers. *Geology* **17**, 1136–1139.

Kar, A., Weaver, B., Davidson, J. & Colucci, M. (1998). Origin of differentiated volcanic and plutonic rocks from Ascension Island, South Atlantic Ocean. *Journal of Petrology* **39**, 1009–1024.

Larson, P. B., Nichols, H. J., Wolff, J. A. & Marti, J. (2001). O and H isotope ratios of syenite blocks in the El Abrigo ignimbrite, Tenerife, Canary Islands: a hydrothermal fingerprint for assimilation. *EOS Transactions, American Geophysical Union* **82**, Fall Meeting Supplement, V12D-1013.

McDermott, F. & Hawkesworth, C. (1991). Th, Pb and Sr isotope variation in young island arc volcanics and oceanic sediments. *Earth and Planetary Science Letters* **104**, 1–15.

Michael, P. J. (1983). Chemical differentiation of the Bishop Tuff and other high-silica magmas through crystallization processes. *Geology* **11**, 31–34.

Moore, R. B. (1990). Volcanic geology and eruption frequency, São Miguel, Azores. *Bulletin of Volcanology* **52**, 602–614.

Moore, R. B. (1991). Geology of three Late Quaternary stratovolcanoes on São Miguel, Azores. *US Geological Survey Bulletin* **1900**, 1–46.

Moore, R. B. & Rubin, M. (1991). Radiocarbon dates for lava flows and pyroclastic deposits on São Miguel, Azores. *Radiocarbon* **33**, 151–164.

Muehlenbachs, K. (1987). Oxygen isotope exchange during weathering and low-temperature alteration. In: Kyser, T. K. (ed.) *Stable Isotope Geochemistry of Low Temperature Processes*. Saskatoon, Sask.: Mineralogical Association of Canada, pp. 162–186.

Palacz, Z. A. & Wolff, J. A. (1989). Strontium, neodymium and lead isotope characteristics of the Granadilla Pumice, Tenerife: a study of the causes of strontium isotope disequilibrium in felsic pyroclastic deposits. In: Saunders, A. D. & Norry, M. J. (eds) *Magmatism in the Ocean Basins*. *Geological Society, London, Special Publications* **42**, 147–159.

Pietruszka, A. J., Carlson, R. W. & Hauri, E. H. (2002). Precise and accurate measurement of ^{226}Ra–^{230}Th–^{238}U disequilibria in volcanic rocks using plasma ionization multicollector mass spectrometry (MC-ICP-MS). *Chemical Geology* **188**, 171–191.

Rehkamper, M. & Halliday, A. N. (1998). Accuracy and long-term reproducibility of lead isotopic measurements by MC-ICPMS using an external method for the correction of mass discrimination. *International Journal of Mass Spectrometry* **181**, 123–133.

Reid, M. R. & Coath, C. D. (2000). *In situ* U–Pb ages of zircons from the Bishop Tuff: no evidence for long crystal residence times. *Geology* **28**, 443–446.

Shotton, F. W., Blundell, D. J. & Williams, R. E. G. (1968). Birmingham University radiocarbon dates, II. *Radiocarbon* **10**, 204.

Shotton, F. W., Blundell, D. J. & Williams, R. E. G. (1969). Birmingham University radiocarbon dates, III. *Radiocarbon* **11**, 266.

Spera, F. J. & Bohrson, W. A. (2001). Energy-constrained open-system magmatic processes I: general model and energy-constrained assimilation and fractional crystallization (EC-AFC) formulation. *Journal of Petrology* **42**, 999–1018.

Staudigel, H., Davies, G. R., Hart, S. R., Marchant, K. M. & Smith, B. M. (1995). Large scale isotopic Sr, Nd and O isotopic anatomy of altered oceanic crust: DSDP/ODP sites 417/418. *Earth and Planetary Science Letters* **130**, 169–185.

Storey, M., Wolff, J. A., Norry, M. J. & Marriner, G. F. (1989). Origin of hybrid lavas from Agua de Pao volcano, São Miguel, Azores. In: Saunders, A. D. & Norry, M. J. (eds) *Magmatism in the Ocean Basins*. *Geological Society, London, Special Publications* **42**, 161–180.

Tegtmeyer, K. J. & Farmer, G. L. (1990). Nd isotopic gradients in upper crustal magma chambers: evidence for *in situ* magma–wall-rock interaction. *Geology* **18**, 5–9.

Todt, W., Cliff, R. A., Hanser & Hoffmann, A. W. (1996). Evaluation of a ^{202}Pb–^{205}Pb double spike for high-precision lead isotope analysis. In: Hart, S. R. & Basu, A. (eds) *Earth Processes: Reading the Isotopic Code*. *Geophysical Monograph, American Geophysical Union* **95**, 429–437.

Turner, S., Hawkesworth, C., Rogers, N. & King, P. (1997). U–Th isotope disequilibria and ocean island basalt generation in the Azores. *Chemical Geology* **139**, 145–164.

Walker, G. P. L. & Croasdale, R. (1970). Two Plinian-type eruptions in the Azores. *Journal of the Geological Society, London* **127**, 17–55.

Walker, R. J., Carlson, R. W., Shirey, S. B. & Boyd, S. B. (1989). Os, Sr, Nd and Pb isotope systematics of southern African peridotite xenoliths: implications for the chemical evolution of subcontinental mantle. *Geochimica et Cosmochimica Acta* **53**, 1583–1595.

Widom, E., Schmincke, H.-U. & Gill, J. (1992). Processes and timescales in the evolution of a chemically zoned trachyte: Fogo A, São Miguel, Azores. *Contributions to Mineralogy and Petrology* **111**, 311–328.

Widom, E., Gill, J. & Schmincke, H.-U. (1993). Syenite nodules as a long-term record of magmatic activity in Agua de Pao volcano, São Miguel, Azores. *Journal of Petrology* **34**, 929–953.

Widom, E., Carlson, R. W., Gill, J. B. & Schmincke, H. U. (1997). Th–Sr–Nd–Pb isotope and trace element evidence for the origin of the São Miguel, Azores, enriched mantle source. *Chemical Geology* **140**, 49–68.

Wolff, J. A. & Palacz, Z. A. (1989). Lead isotope and trace element variation in Tenerife pumices: evidence for recycling within an ocean island volcano. *Mineralogical Magazine* **53**, 519–525.

Wolff, J. A., Balsley, S. D. & Gregory, R. T. (2002). Oxygen isotope disequilibrium between quartz and sanidine from the Bandelier Tuff, New Mexico, consistent with a short residence time of phenocrysts in rhyolitic magma. *Journal of Volcanology and Geothermal Research* **116**, 119–135.

Wörner, G., Staudigel, H. & Zindler, A. (1985). Isotopic constraints on open system evolution of the Laacher See magma chamber (Eifel, West Germany). *Earth and Planetary Science Letters* **75**, 37–49.